THE JOURNAL OF PHYSICAL CHEMISTRY C

Article

pubs.acs.org/JPCC

Adsorption and Separation of $N_2/CH_4/CO_2/SO_2$ Gases in Disordered Carbons Obtained Using Hybrid Reverse Monte Carlo Simulations

Xuan Peng,*[,†] Surendra Kumar Jain,[‡] and Jayant Kumar Singh[‡]

[†]College of Information Science and Technology, Beijing University of Chemical Technology, Beijing 100029, P R China

[‡]Department of Chemical Engineering, Indian Institute of Technology Kanpur, Kanpur, 208016, India

Supporting Information

ABSTRACT: Adsorption and separation of gases in porous carbon models are studied using molecular simulations. We use three porous carbon models (named as cs400, cs1000, and cs1000a) developed in a previous work obtained from Hybrid Reverse Monte Carlo simulations. The density of carbon atoms as well as the presence of heteroatoms (hydrogen and oxygen) differ between the three carbon models. Gas adsorption in the carbon models were studied using Grand Canonical Monte Carlo simulations. We found that cs1000 sample (with highest carbon density) shows the largest separation ability for N_2/CH_4, CH_4/CO_2, and N_2/CO_2 systems. cs1000a sample (with larger pore width up to 1.2 nm) shows higher selectivity for SO_2/N_2 and SO_2/CO_2 systems. We also studied the influence of surface chemistry (presence of carbonyl and carboxyl groups) in the porous carbon models on adsorption and separation of gases. We found that the presence of carbonyl and carboxyl groups has a significant effect on the adsorption and separation of polar gas molecules. Interestingly, the presence of functional groups does not seem to have much impact on SO_2/CO_2 separation at moderate to high pressures for carbonyl functional groups. For carboxyl functional groups, this is not the case, and the selectivity curves remain flat or decrease slightly at moderate to high pressures. We found increasing selectivity for all binary gas systems except for the N_2/CH_4 system, which is expected, as both the gases are nonpolar. For all binary gas systems studied, the maximum selectivity was found for SO_2/N_2 system.

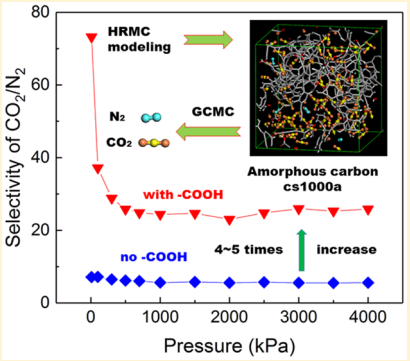

INTRODUCTION

Porous carbons are disordered materials with a heterogeneous pore structure. These materials have found widespread use in industry owing to their excellent surface activity. The surface activity comes from the high density of carbon atoms at the surface.[1] These materials have found application in separation and storage of gases[2,3] and also as a means to store methane and hydrogen.[4,5] The adsorption of gases in activated carbons is mainly dependent on the adsorbate gases. The adsorption of nonpolar gases is dependent mainly on pore size and the density of carbon atoms. However, the adsorption of polar gases is dependent on the nature of chemical groups present in the activated carbons.

Emission of CO_2 and SO_2 has become an environmental concern and has drawn widespread attention.[6−8] Numerous studies have been conducted to separate and capture CO_2[9−11] and SO_2[12−17] from flue gas. To understand CO_2 and SO_2 capture, numerous adsorbents have been reported in the literature using activated carbons, carbon nanotubes, zeolites, and metal organic framework.[18−36] Among these adsorbents, carbon-based materials have shown great promise due to their better adsorbent qualities, effective surface modification, and functionalization.[37−39] Porous carbons also possess high specific surface area, moderate heat of adsorption, low-cost preparation, relatively easy regeneration, and less sensitivity to the humidity effect than the other CO_2-philic materials. A number of techniques have been developed to capture SO_2 and CO_2 from flue gas. Adsorption technique has emerged a powerful technique to capture these harmful gases. A desirable adsorbent material should have high selectivity for these harmful gases, have high storage capacity, and should be easily regenerated. Porous carbons have emerged as a promising adsorbent to capture these harmful gases. Numerous studies have been undertaken to tune the pore size and chemical composition (presence of functional groups) of porous carbons for optimal storage and capture of these gases. The major component of natural gas is CH_4. It is well known that the presence of CO_2 and N_2 in natural gas leads to less efficiency of natural gas as a fuel. Therefore, the separation of CO_2/CH_4 and N_2/CH_4 mixture is highly desirable. Also, the presence of CO_2 in natural gas will degrade the transportation and storage systems of natural gas.[40−45] By carefully selecting adsorbent, CO_2 can be separated from CH_4 depending on their binding affinity to the adsorbent.

The nature of interactions in porous materials is hard to elicit from experiments because of the myriad of factors that affect adsorption, including functional group concentration and topology,[46] finite extent of pores,[47] and pore connectivity.[48,49] Thus molecular simulation plays an important role in examining

Received: February 27, 2017
Revised: June 1, 2017
Published: June 1, 2017

DOI: 10.1021/acs.jpcc.7b01925
J. Phys. Chem. C 2017, 121, 13457−13473

these above-mentioned factors, affecting adsorption and dynamics of fluid molecules. However, to understand the factors affecting adsorption and transport properties of confined fluids, a realistic model of the porous material sample and reliable interaction potential between the adsorbent and fluid molecules are needed. A large number of studies have gone into developing accurate interatomic potentials using both experiments and first-principle calculations[50] (and references therein). However, our understanding of the underlying microstructure of porous carbons is still not clear.

In a recent work, we developed molecular models for three microporous carbons (named cs400, cs1000, and cs1000a) using Hybrid Reverse Monte Carlo (HRMC) method.[51] Our models reveal a heterogeneous pore structure that interconnected in a complex way. The isosteric heat of adsorption for argon adsorption predicted from those models was in good agreement with experiments.[52] We have developed molecular models of cs400, cs1000, and cs1000a in a previous study.[51] The radial distribution functions from HRMC simulations match very well the experimental ones. We show the simulated and experimental radial distribution functions in Figures S1−S3 of the Supporting Information. In HRMC, we also used an energy penalty term that makes sure we do not have unrealistic features in the HRMC carbon models. Thus the HRMC procedure produces a 3D carbon model that matches the radial distribution functions with that of experiments and minimizes the energy. We also calculated the neighbor distributions and bond-angle distributions of sp, sp2, and sp3 carbons and found that bond-angle distributions are according to the carbon hybridization. We also calculated the ring statistics and found that our HRMC carbon models contain five-, six-, and seven-membered rings and statistically no three- or four-membered rings. We further calculated the bond-angle distributions in five-, six-, and seven-membered and found those to be consistent with the actual values. This shows that our HRMC models can capture the correct chemistry at the local level while still matching the experimental radial distribution functions. We also calculated the geometric pore-size distribution in the three HRMC carbon models and found that the carbon models contain micropores (as present in normal microporous carbon materials), and the distribution is different for each case. In another study,[52] we computed the adsorption isotherms and isosteric heats of adsorption, in our HRMC models, using Grand Canonical Monte Carlo (GCMC) simulations. Our simulated isosteric heat is in good agreement with that of experiments. This shows that the pore heterogeneity is captured well by our models. By visual inspection of the carbon models, we found that the pore morphology and topology are different from standard slit-pore models. In another study,[53] we found that the dynamics of argon inside a disordered carbon model is different from slit-pore model. While the self-diffusivity of argon in slit-pore models decreases with loading, it exhibits a maximum for disordered porous carbon model. Such a nonmonotonous behavior of self-diffusivities in disordered porous carbon models can be explained by their surface (energetic) heterogeneities. In a recent study,[54] the authors found good agreement between experimental and simulated selectivity between CO_2 and CH_4. The carbon model used was developed by one of us using a constrained Reverse Monte Carlo (RMC) method.[55] The authors added −OH groups to the carbon models and noted that adding functional groups is necessary to accurately predict the selectivities in the hydrophobic carbon models. HRMC simulations have been used by other researchers[56,57] to model successfully disordered microporous carbons prepared experimentally via different routes. All of these above studies show that HRMC is able to capture the pore and surface heterogeneity present in the real microporous carbons.

Thus we use those HRMC carbon models in this work to predict the adsorption and selectivity of a number of gases. It is widely known that the adsorption and transport properties of fluid (mainly polar) molecules are governed by the presence of functional groups (those containing oxygen), mainly at low pressure (and thus at low loadings).[58,59] The presence of functional groups enhances the adsorption and separation of carbon materials. These functional groups interact via multipole interaction with the gas molecules and hence enhance the binding of the gas to the adsorbent. It is very difficult to identify and quantify the functional groups present in the real adsorbent by experiments owing to the complex pore structure of the adsorbent. Molecular simulation plays an important role, as we can study the effect of the nature and concentration of the polar groups on adsorption and separation. Consequently, it is pertinent to add functional groups to the carbon models to realistically predict adsorption and diffusion properties. A number of papers have been published in the past few years where researchers have added functional groups to the graphite slit-pore model. The functional groups are normally added to the surface of the slit pore or at the edges of the graphite planes. Ayappa and coworkers[50] studied the effect of edge-functionalized graphene nanoribbons, of a number of functional groups, on the selectivity of CO_2/N_2 mixture using GCMC simulations. They found that the presence of functional groups, especially COOH, increases the selectivity of CO_2 over N_2 as compared with other functional groups (OH, NO_2, NH_2, CH_3). Wilcox and coworkers[60] studied the effect of oxygen-containing functional groups on the adsorption of mixtures of CO_2/CH_4 and CO_2/N_2. They found that due to the presence of functional groups CO_2 adsorbs preferentially at these sites as compared with CH_4 and N_2. Thus the selectivity of CO_2 over CH_4 and N_2 was found to be much higher, especially in the low-pressure regime. They concluded that by tuning the surface chemistry (having a significant amount of COOH groups) of the porous carbons, a higher selectivity of CO_2 over other gases could be achieved. Shen and coworkers[61] studied the effect of edge functionalization of graphene segments on the adsorption of CO_2/CH_4 mixture using density functional theory (DFT) and GCMC simulations. The functional groups studied are NH_2, COOH, OH, and H groups. They found that edge functionalization had a significant effect on CO_2 adsorption but had less influence on CH_4 adsorption. They also found that temperature had negative influence on adsorption but no obvious influence on the selectivity. Steriotis and coworkers[62] studied the influence of functional groups on the adsorption of CO_2 and N_2. They used epoxy and hydroxyl groups with different concentrations on graphite surfaces of slit pore. They found that the adsorption increases dramatically with the introduction of the surface functional groups, and the adsorption isotherm gets smoother as compared with the pristine graphitic slit pore. In a recent work, Maurya et al.[63] studied the adsorption and separation of $SO_2/CO_2/N_2$ gases in edge-functionalized graphene nanoribbons. They found that the adsorption and selectivity of SO_2 increase with increased functionalization, mainly at low pressure.

The above-mentioned simulation studies have been reported with attached functional groups on slit-pore carbon models.

DOI: 10.1021/acs.jpcc.7b01925
J. Phys. Chem. C 2017, 121, 13457−13473

Table 1. Force-Field Parameters for Adsorbates and Adsorbents

adsorbate	atom	σ (Å)	ε/k_b (K)	q (e)	angle (deg)	bl (Å)[a]
N_2	N	3.31	36.0	−0.482	180	1.1
	com			0.964		
CH_4		3.73	148.0			
CO_2	C	2.8	27.0	+0.7	180	1.16
	O	3.05	79.0	−0.35		
SO_2	S	3.585	154.4	+0.470	119.5	1.4321
	O	2.993	62.3	−0.235		
adsorbent	C	3.36	28.0			
	H	2.42	15.08			
−C═O	C[b]			+0.5		
	O	2.96	105.8	−0.5		
−COOH	C[b]			+0.08		
	C	3.75	52.0	+0.55		
	O(═C)	2.96	105.7	−0.5		
	O(−H)	3.0	85.6	−0.58		
	H(−O)			+0.45		

[a]bl is the bond length. [b]Carbon atom of HRMC carbon matrix that connects the functional groups.

However, not much literature is available on the realistic carbon models with attached functional groups. Recently, De Weireld and coworkers[64] have reported experimental measurements and GCMC simulations of CO_2, CH_4, and water in porous carbons. The porous carbon model used in their study is a realistic molecular model obtained from HRMC simulations. (The HRMC molecular model for carbon was originally developed by Jain et al.[55]) The authors added random H and OH functional groups to the original HRMC model to study the effect of functionalization on the adsorption properties of gas molecules. They found qualitative agreement between experiments and simulation at low pressure. The authors pointed out that the discrepancy between experiment and simulation was due to the insufficient number of functional groups and also due to the absence of other polar groups normally present in the porous carbons. Thus they concluded that the carbon model used was not hydrophilic enough to describe adsorption in real active carbons. In a recent work, Halder et al.[65] have studied the influence of functional groups in CMK-5 models on adsorption and separation of $CO_2/N_2/CH_4$ gases. They found that the functionalization increases the selectivity of CO_2 over other gases. Furmaniak et al.[66] studied the influence of functional groups on SO_2 adsorption in virtual porous carbons. They used only carbonyl functional groups in their study and found that the electrostatic interaction of carbonyl with SO_2 molecules resulted in an increase in adsorption of SO_2 and that the pore-filling pressure decreases with increasing functional groups. Wang et al.[20] also studied the influence of carbonyl functional groups on the separation of binary mixture containing $SO_2/CO_2/N_2/H_2S$ gases in carbon nanotubes. They found that the presence of carbonyl groups enhances the adsorption of SO_2 compared with other gas molecules. All of this literature points to the importance of attached functional groups to the carbon models to capture the real chemistry between the fluid molecules and the adsorbent (carbon matrix).

In our previous work,[67] we have extensively investigated 18 kinds of porous materials from carbons, zeolites, and metal organic frameworks (MOFs) for desulfurization and decarburization of the biogas, natural gas, and flue gas. However, the above-mentioned porous materials are highly ordered crystal materials, which may give different adsorption properties from the disordered carbons used here. Therefore, in this work we report results from GCMC simulations of gases in the pristine carbon models and carbon models with attached carbonyl (−C═O) groups and carboxyl groups (−COOH) obtained from HRMC simulations. We have studied the presence of carbonyl and carboxyl groups, as it was shown by Jorge et al.[46] that the nature of functional groups is of little significance for physisorption. Carbonyl functional groups have been used by researchers before to understand adsorption in porous carbons.[20,66] We investigate the presence of hydrogen atoms and carbonyl and carboxyl functional groups on the adsorption properties and selectivity of gases. We performed GCMC simulation of gases in HRMC models containing (a) only carbon atoms, (b) both carbon and hydrogen atoms, (c) carbon, hydrogen, and carbonyl functional groups, and (d) carbon, hydrogen, and carboxyl functional groups. We further studied the separation of gases from equimolar gaseous mixtures. We also report the effect of carbonyl and carboxyl functional groups on the separation of gaseous mixtures.

COMPUTATIONAL DETAILS

Models of Microporous Carbons. Microporous carbons used in this work have been prepared using a HRMC method, in a previous work.[51,52] Normal RMC method includes generating atomistic models that match the structural data (normally pair correlation function or structure factor) of the real materials. However, the RMC method suffers from a drawback; that is, the models obtained from RMC are not unique if many body forces exist in the system. To overcome the drawback, in HRMC, an energy penalty term is added so that the resultant model obtained matches the pair correlation function of the system and also has low energy.

Here we used atomistic models for three carbon samples obtained from Saccharose coke.[51,52] The samples are named as cs400, cs1000, and cs1000a. cs400 was obtained by heating coke at 400 °C, cs1000 was obtained by heating coke at 1000 °C, and cs1000a was obtained by activating cs1000 sample. The cs1000 sample has the highest density, and cs1000a has the lowest density. The number of carbon atoms is the highest in cs1000 and lowest in cs1000a models. In generating the atomistic models, we considered both carbon and hydrogen atoms in our simulation box. The number of carbon atoms and hydrogen atoms was obtained from the

DOI: 10.1021/acs.jpcc.7b01925
J. Phys. Chem. C 2017, 121, 13457−13473

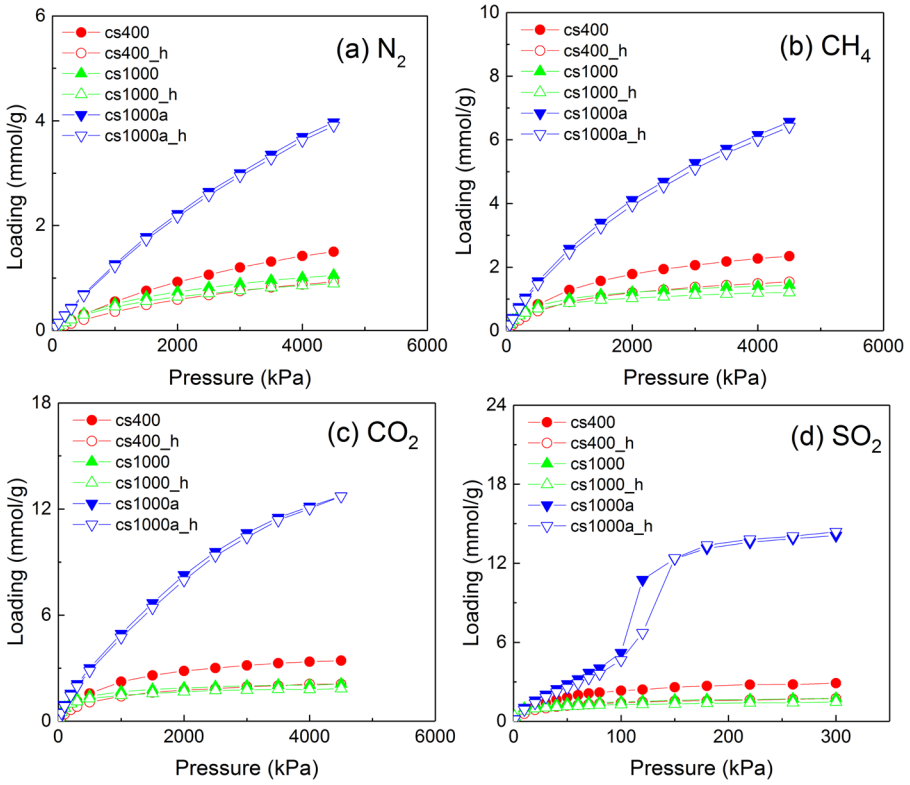

Figure 1. Absolute adsorption isotherms of pure gases in carbon materials at 303 K.

density and H/C ratio, determined from experiments. During the course of HRMC simulation, both carbon and hydrogen atoms were moved. More details of generating the models can be found here.[51,52] Our models reproduced the experimental pair correlation function very well and also captured correct chemistry of the carbon atoms at the local level. The pore-size distribution[51,52] of the carbon models revealed that cs400 and cs1000 have very narrow micropores (3.5−7 Å), whereas cs1000a contains pores ranging until 12 Å. The isosteric heat of adsorption predicted by our models was found to be in good agreement with the experiments,[52] which shows that our models capture the energetic heterogeneity present in the real materials with complex pore morphology and topology. This gives us confidence in using these models to study the adsorption and separation of gases.

Adding Carbonyl Functional Groups to the HRMC Models. In this work, we add functional groups to the HRMC models.[51] We consider both carbonyl and carboxyl groups. The potential parameters for both functional groups are taken from the literature of Zeng et al.[68] It has been shown by Jorge et al.[46] that the nature of the oxygen functional groups is not as critical as the concentration of the functional groups. Carbonyl functional group has been used before in porous carbon models.[20,66] Furmaniak et al.[66] studied the influence of carbonyl groups, in virtual porous carbon models, on SO_2 adsorption. Wang et al.[20] studied the influence of carbonyl groups, in carbon nanotubes, on separation of gases. Both of these studies attached an oxygen atom to a carbon atom in the carbon matrix for carbonyl groups. Thus only oxygen atom was attached to an existing carbon atom to generate a carbonyl group. We also followed a similar procedure to obtain carbonyl functional groups. The recipe to add carbonyl (−C═O) groups is as follows: We first find carbon atoms that have one or more hydrogen neighbors. We then randomly select a carbon atom (having hydrogen neighbors) and randomly replace one of the hydrogen atom neighbors with an oxygen atom. The distance between the carbon atom and oxygen atom is that of C═O distance. Care is taken that the oxygen atom being added does not overlap with other carbon, hydrogen, or oxygen atoms. The carbon atom to which the oxygen is being attached is treated as the carbon of the −C═O (carbonyl group). The charge on the oxygen atom is (−0.5e), and the charge on the carbon of the −C═O group has a charge of +0.5e. This procedure makes sure that the oxygen atom is not overlapped with any of the carbon and hydrogen atoms present in the system. Thus the total number of atoms present in the models remains the same. Some of the hydrogen atoms are converted into oxygen (of carbonyl group) atoms. These carbon atoms having hydrogen neighbors may be thought of as edge carbon atoms in a graphene segment.

We investigated the effect of carbonyl functional groups on the separation of gases for all three carbon samples. The number of carbonyl groups added is as follows: (a) cs400_28:28 carbonyl functional groups added to cs400 sample, (b) cs400_84:84 carbonyl functional groups added to cs400 sample, (c) cs400_140:140 carbonyl functional groups added to cs400 sample, (d) cs1000_28:28 carbonyl functional groups added to cs1000 sample, (e) cs1000_84:84 carbonyl functional groups added to cs1000 sample, and (f) cs1000a_28:28 carbonyl functional groups added to cs1000a sample. We have added more carbonyl functional groups to cs400 because it contains the highest number of hydrogen atoms and cs1000a has the lowest number of hydrogen atoms.

Adding Carboxyl Functional Groups to the HRMC Models. The recipe adding −COOH groups is as follows: There are some carbon atoms with one carbon neighbor. We add a double-bond oxygen (═O) and −OH group to those carbon atoms. To add a double-bonded oxygen (═O), we

DOI: 10.1021/acs.jpcc.7b01925
J. Phys. Chem. C 2017, 121, 13457−13473

Table 2. Summary of Structural Properties for Carbon Materials[a]

materials	ρ_f (g/cm^3)	V_{free} (cm^3/g)	ϕ
cs400	1.056	0.442	0.466
cs400_h	1.103	0.369	0.407
cs400_28	1.147	0.349	0.399
cs400_84	1.236	0.311	0.384
cs400_140	1.326	0.277	0.368
cs400_28cooh	1.199	0.322	0.386
cs400_48cooh	1.264	0.295	0.373
cs1000	1.481	0.231	0.342
cs1000_h	1.499	0.216	0.324
cs1000_28	1.544	0.205	0.316
cs1000_84	1.633	0.185	0.302
cs1000_23cooh	1.579	0.195	0.308
cs1000a	0.723	0.912	0.659
cs1000a_h	0.728	0.897	0.653
cs1000a_28	0.773	0.831	0.642
cs1000a_24cooh	0.811	0.774	0.628

[a]Lattice parameters at x, y, and z axes are equal to 25 Å for all materials, ρ_f is the framework density, V_{free} is the free pore volume of the available void volume to fluid molecules, calculated by a Monte Carlo integration with the reentrant surface definition,[69] and ϕ is the porosity expressed by the ratio of the free volume of adsorbent accessible to gas molecules to the adsorbent volume.

chose a random point on a sphere of the desirable radius (same as C═O distance) and added the oxygen atom. Care is taken that the added oxygen is not overlapping with other atoms. Similarly, to add a hydroxyl group (−OH) group we chose a random point on a sphere of the desired radius (same as C−OH) distance an add the oxygen atom and similarly add the hydrogen atom to the oxygen atom. We remove any hydrogen neighbors that these carbon atoms (with one carbon neighbor, which we treat as COOH group) have. We then relax the HRMC models with attached functional groups (−COOH) using the REBO potential developed for carbon−oxygen−hydrogen systems.[69,70] During the relaxation process, carbon atoms are held fixed and the hydrogen and oxygen atoms are allowed to move.

We investigated the effect of carboxyl functional groups on the separation of gases for all three carbon samples. The number of carboxyl groups added is as follows: (a) cs400_28cooh: 28 carboxyl functional groups added to cs400 sample, (b) cs400_48cooh: 48 carboxyl functional groups added to cs400 sample, (c) cs1000_23cooh: 23 carboxyl functional groups added to cs1000 sample, and (d) cs1000a_24cooh: 24 carboxyl functional groups added to cs1000a sample. We have a smaller number of carboxyl groups as compared with carbonyl groups to our carbon samples because the number of carbon atoms with one carbon neighbor is less in all of those carbon samples, which is not surprising.

Grand Canonical Monte Carlo Simulations. Using the HRMC simulation-built carbon atomic models, we further performed GCMC[71] simulations to investigate adsorption and separation of binary gases in these materials. During the simulations, the adsorbents were treated as a rigid material with atoms frozen. The periodic boundary conditions were imposed in three dimensions. The LJ and electrostatic potentials were truncated at a cutoff radius of 12.5 Å without long-range corrections. The fluid−fluid interactions of the species are composed of the LJ and electrostatic interactions. We used the TraPPE force field[72,73] to describe the interaction potentials of CH_4, N_2, and CO_2, where CH_4 is regarded as a spherical one-site geometry, and CO_2 is represented by a linear three-site model with the C−O bond length of 1.16 Å. The partial point

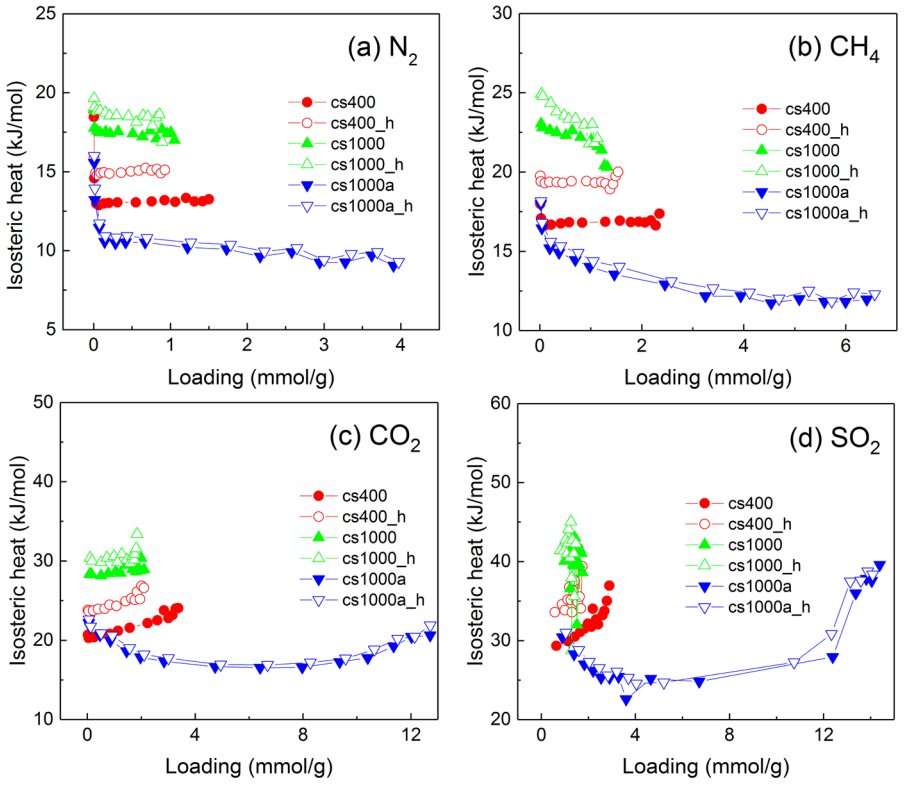

Figure 2. Isosteric heats of pure gases in carbon materials at 303 K.

DOI: 10.1021/acs.jpcc.7b01925
J. Phys. Chem. C 2017, 121, 13457−13473

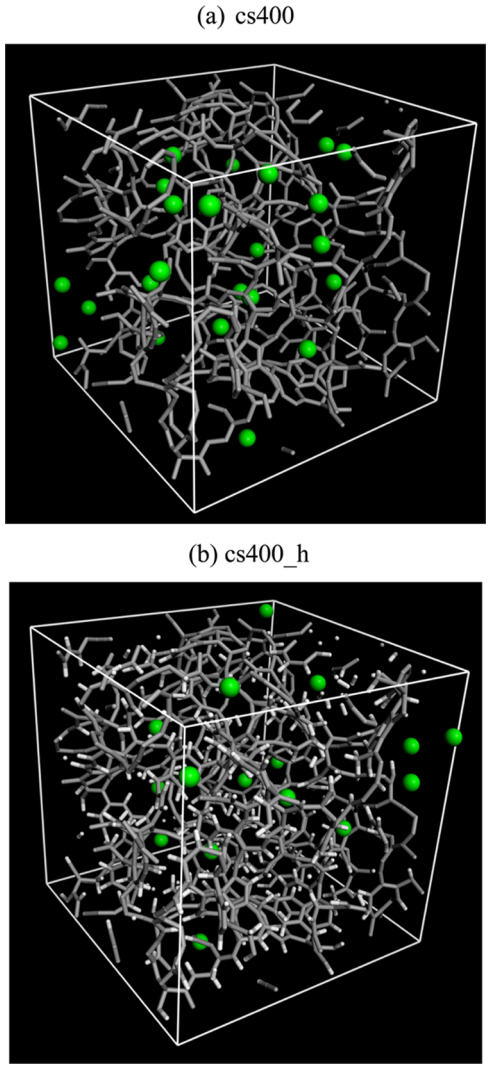

Figure 3. Adsorption configurations of CH_4 in porous materials at 303 K and 4500 kPa.

charge on the C atom is +0.7e, and electric neutrality is maintained by the partial charge of −0.35e on O atom. For N_2, each N atom is modeled by a LJ site separated by the experimental bond length of 1.1 Å. The point charge of −0.482 e is placed on each LJ site to reproduce the gas-phase quadrupole moment of N_2, and a point charge of +0.964 e was placed at the center of mass (COM) of the molecule to maintain charge neutrality. Similarly, in Ribeiro's potential model[67,74] for SO_2 molecule, the S−O bond length and the O−S−O bond angle are 1.4321 Å and 119.5°, and the partial charges on S and O atoms are +0.470*e* and −0.235*e*. All of the potential parameters are given in Table 1 and the Lorentz−Berthelot combining rules are used to calculate the cross-interaction parameters.

To accelerate the simulations, a 3D tabular table of interactions between adsorbate and adsorbent is precalculated with a grid spacing of 0.2 Å. To obtain accurate ensemble averages in GCMC simulations, a total number of 2×10^7 configurations was generated for each pressure point, where the first 1×10^7 configurations were discarded to guarantee equilibration, and the second one was divided into 20 blocks to calculate the ensemble average. For CH_4 with a spherical geometry, only three types of moves, viz., translation, insertion, and deletion, are attempted, whereas for other molecules an additional rotation move is implemented. The normal move acceptance probability is transformed to relate the component fugacity of bulk phase by Peng−Robinson equation of state.[75]

To investigate the separation ability of porous material for gas mixtures, we defined the adsorption selectivities as follows

$$S_{i/j} = \frac{x_i/x_j}{y_i/y_j} \tag{1}$$

where $S_{i/j}$ refers to the selectivity of the first component i over the second component j. For the ternary mixture such as N_2−CO_2−SO_2, CO_2 and SO_2 are combined into one pseudo-component, and the selectivity of (CO_2 + SO_2) over N_2 is calculated according to the above equation. More details of the calculations of adsorption selectivity mixtures and isosteric heat are referred to our previous work.[76]

IAST Prediction for Adsorption of Binary Mixture. It is interesting to compare the binary mixture adsorption from molecular simulation and Ideal Adsorbed Solution Theory (IAST).[76,77] We adopted the dual-site Langmuir−Freundlich (DSLF) adsorption model[42,76] to correlate the pure-component equilibrium data from molecular simulations. The DSLF model is given by

$$N^\circ(f) = \frac{N_1 k_1 f^{n_1}}{1 + k_1 f^{n_1}} + \frac{N_2 k_2 f^{n_2}}{1 + k_2 f^{n_2}} \tag{2}$$

where f is the fugacity of bulk gas at equilibrium with adsorbed phase and N_i, k_i, and n_i are model parameters of maximum adsorption amount at site i (i = 1 or 2), the affinity constant, and the deviation from the simple Langmuir equation, respectively.

On the basis of the available DSLF model parameters of pure gas adsorption, we further predicted the multicomponent adsorptions with IAST, where the adsorbed solutions are assumed to be ideal and all activity coefficients in the adsorbed phase are unity. When adsorption equilibrium is reached between adsorbed phase and gas phase, we obtained[76,77]

$$P y_i \phi_i = x_i f_i^\circ(\pi) \tag{3}$$

where f_i° is the fugacity of the equilibrium gas phase corresponding to the spreading pressure π for the adsorption of pure gas i, ϕ_i is the gas fugacity coefficient of component i calculated by PR EOS, and x_i and y_i are the molar fraction of component i at adsorbed and bulk phases, respectively. The binary gas mixing process at constant spreading pressure π is indicated by[76,77]

$$\int_0^{f_1^\circ} N_1^\circ(f_1)\, \mathrm{d} \ln f_1 = \int_0^{f_2^\circ} N_2^\circ(f_2)\, \mathrm{d} \ln f_2 \tag{4}$$

where the single-component adsorption loading and selectivity are computed by numerical integration and root exploration.

RESULTS AND DISCUSSION

We studied the adsorption and separation of gases in three different versions of carbon models (for the samples: cs400, cs1000, and cs1000a). These are denoted as follows in the rest of the paper: cs400 contains only carbon atoms, cs400_h contains both carbon and hydrogen, cs400_28 contains carbon, hydrogen, and 28 carbonyl groups, and cs400_28cooh contains carbon, hydrogen, and 28 carboxyl groups. Similarly, for cs1000 and cs1000a models we have carbon-only, carbon−hydrogen,

DOI: 10.1021/acs.jpcc.7b01925
J. Phys. Chem. C 2017, 121, 13457−13473

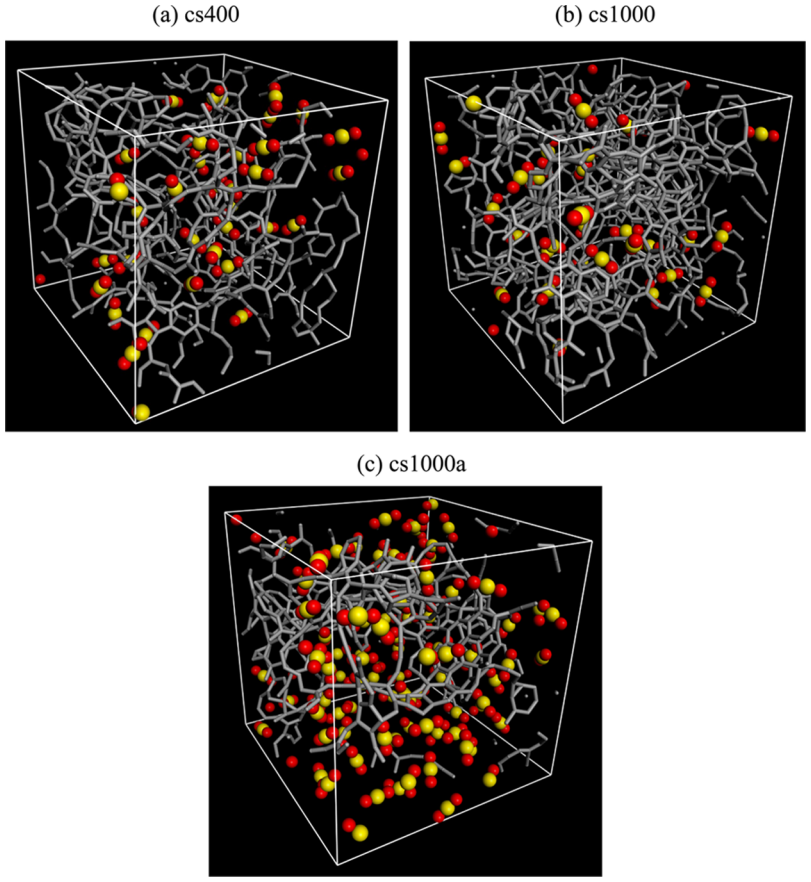

Figure 4. Adsorption configurations of CO_2 in porous materials at 303 K and 300 kPa.

carbon−hydrogen, and carbonyl groups and carbon−hydrogen and carboxyl groups.

Adsorption of Pure Gases. Figure 1 shows the absolute adsorption isotherms of pure gases in carbon materials at 303 K. We can see that for all of the species, cs1000a and cs1000a_h show much higher adsorption amounts than other carbon materials. For instance, the uptake of CO_2 in cs1000a is about four times that of cs400, approaching 12 mmol/g at 4500 kPa. This is because cs1000a has a larger pore volume of 0.912 cm^3/g to accommodate more adsorbate molecules, compared with that of 0.442 cm^3/g for cs400 (see Table 2). Moreover, CO_2 has the largest loading at 4500 kPa, followed by CH_4 and N_2. The amount adsorbed for carbon-only and carbon−hydrogen models is approximately the same for CO_2, CH_4, and N_2 gases for cs1000 and cs1000a models. However, the carbon-only model of cs400 sample shows more gas intake, as compared with carbon hydrogen model of cs400_h (Figure 3). From Figure 2, we can also observe that those species with a higher heat of adsorptions have larger uptakes. In particular, at low pressures, there is a strong correlation between loading and heat of adsorption. The higher uptakes are attributed to the stronger binding energy between the guest molecules and frameworks. For cs1000a/cs1000a_h, the strongly adsorbed species such as CO_2 and SO_2 exhibit a local minimum of the adsorption heats. As expected, the contribution of the solid−fluid interactions dominates at low loadings, while the contribution from the fluid−fluid interactions is of more importance at high adsorption densities. As a result, the local minimum of isosteric heats appears due to the competitive balance of the isosteric heats contributed by the solid−fluid interactions and the fluid−fluid interactions. Note that for all of the species cs1000a and cs1000a_h have the lowest isosteric heats despite the greatest loadings. This is due to the smaller number of carbon atoms (which results in less dispersion interaction between solid and fluid molecules) in cs1000a as compared with cs400 and cs1000. Furthermore, cs1000 and cs1000_h have the highest heats of adsorption. The inconsistence for the variations of loading and isosteric heat results from the material structure and molecular adsorption state. Figure 4 shows the snapshots of CO_2 in cs400, cs1000, and cs1000_a at 4500 kPa and 303 K. We can see that for cs1000a, the smallest material density caused by the large pore volume will definitely reduce the isosteric heat of adsorption, whereas the carbon networks of cs1000 are distributed more densely (due to the higher carbon density of cs1000), and accordingly their isosteric heats are the largest ones. The order of isosteric heat for the adsorbed gases shows the following order for all carbon models: $SO_2 > CO_2 > CH_4 > N_2$. This is not surprising because the interaction strength between gases and the carbon matrix also follows the same order. There is a marked difference between the isosteric heat for a particular adsorbent for all of the gases studied. This difference in isosteric heat between the gases is >5 kJ/mol for all of the adsorbents, suggesting that the porous carbons have preference of one gas over other and can be used for separation of gases.

Separation of Binary Mixture. Figures 5−9 show the pairwise adsorption selectivities and the single-component isotherms of CH_4−CO_2, N_2−CH_4, N_2−CO_2, N_2−SO_2, and CO_2−SO_2 systems in the cs400/cs400_h, cs1000/cs1000_h, and cs1000a/cs1000a_h materials. We find that cs1000a/cs1000a_h

DOI: 10.1021/acs.jpcc.7b01925
J. Phys. Chem. C 2017, 121, 13457−13473

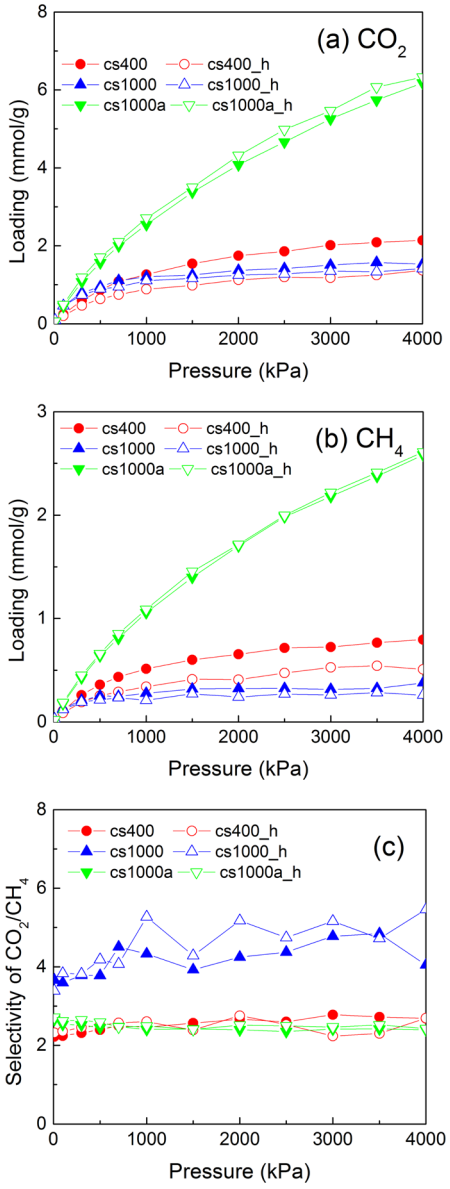

Figure 5. Adsorption isotherms and selectivity of equimolar CH_4−CO_2 mixture at 303 K.

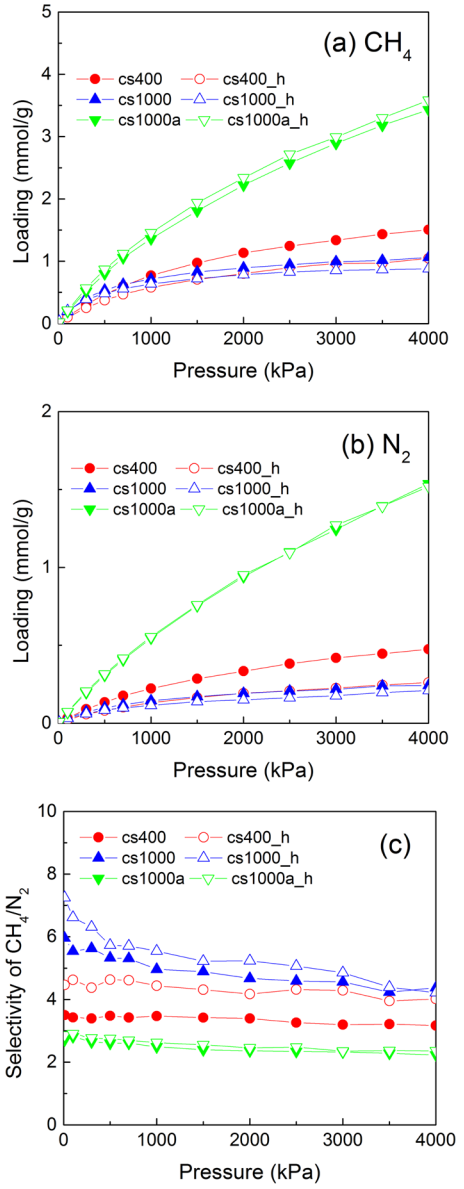

Figure 6. Adsorption isotherms and selectivity of equimolar N_2−CH_4 mixture at 303 K.

materials occupy the greatest adsorption capacities for all of the binary mixtures. For CH_4−CO_2, N_2−CH_4, and N_2−CO_2 systems, cs1000/cs1000_h shows the best separation performance, while for N_2−SO_2 and CO_2−SO_2 systems, cs1000a/cs1000a_h have the largest adsorption selectivities. For the former, the confinement of the cs1000/cs1000_h sample with highest carbon density plays an important role to affect separation for the nonpolar molecules in the N_2−CH_4−CO_2 system. For the latter, the large pore size of the cs1000a/cs1000a_h sample can accommodate larger SO_2 molecules and thus improve the separation for the gas mixtures containing sulfide. As reported in the literature, the optimum pore size for SO_2/N_2 separation is 0.81 nm and that for SO_2/CO_2 separation is 1.09 nm.[20] cs1000a/cs1000a_h models have pore size ranging to 1.2 nm, and cs400/cs1000 models have pore size up to 0.7 nm. This explains the greater selectivity of cs1000a/cs1000a_h models containing SO_2 molecules. Furthermore, the selectivity curves exhibit apparently different behaviors with the increase in pressure, such as monotonically ascending for CH_4−CO_2, descending for N_2−CH_4, constant for N_2−CO_2, and fluctuating for N_2−SO_2 in cs1000a/cs1000a_h. For CO_2/CH_4 system, cs1000/cs1000_h shows the highest selectivity (~4.8), which is consistent with the results reported in the literature for activated carbons.[78] For CH_4/N_2 system, cs1000_h/cs1000 has the highest selectivity. The selectivity varies from 7.5 at low pressure to 4.2 at high pressure. Interestingly, the presence of carbon−hydrogen models shows a slight higher selectivity than the carbon-only models. It has been reported in the literature that the smallest pore where CO_2 can adsorb is 0.57 nm and the smallest pore for CH_4 adsorption is 0.61 nm. Thus cs1000/cs400 with pore size up to 0.7 nm shows higher selectivity compared with cs1000a, which has higher pore size. This can be shown from the isosteric heat for CO_2/CH_4 gases, where cs1000 has higher values compared with cs1000a and cs400. For CO_2/N_2 system, the selectivity of cs1000/cs1000_h models is higher than that of cs400 and cs1000a samples, which can be explained by the amount adsorbed for the CO_2/N_2 mixture. The amount adsorbed for

DOI: 10.1021/acs.jpcc.7b01925
J. Phys. Chem. C 2017, 121, 13457−13473

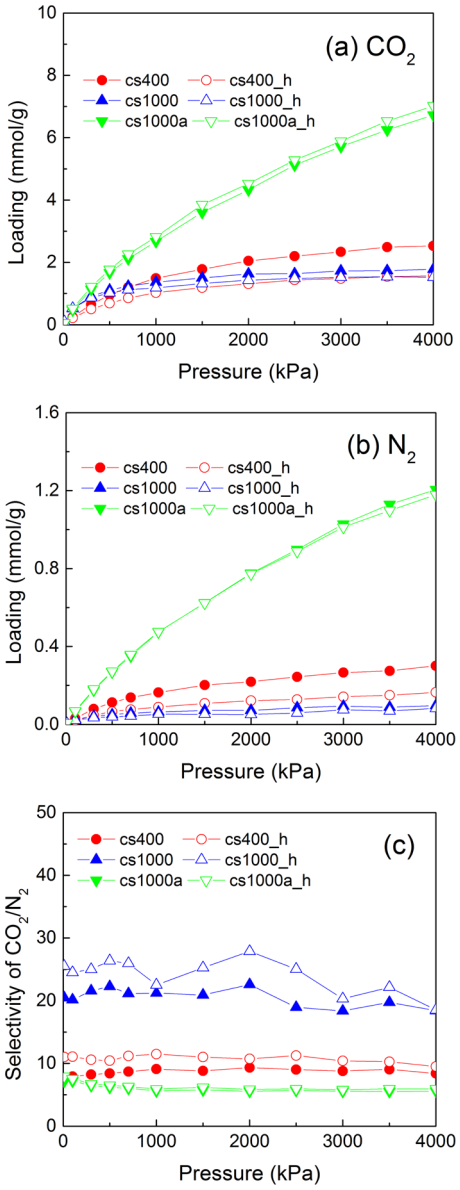

Figure 7. Adsorption isotherms and selectivity of equimolar N_2−CO_2 mixture at 303 K.

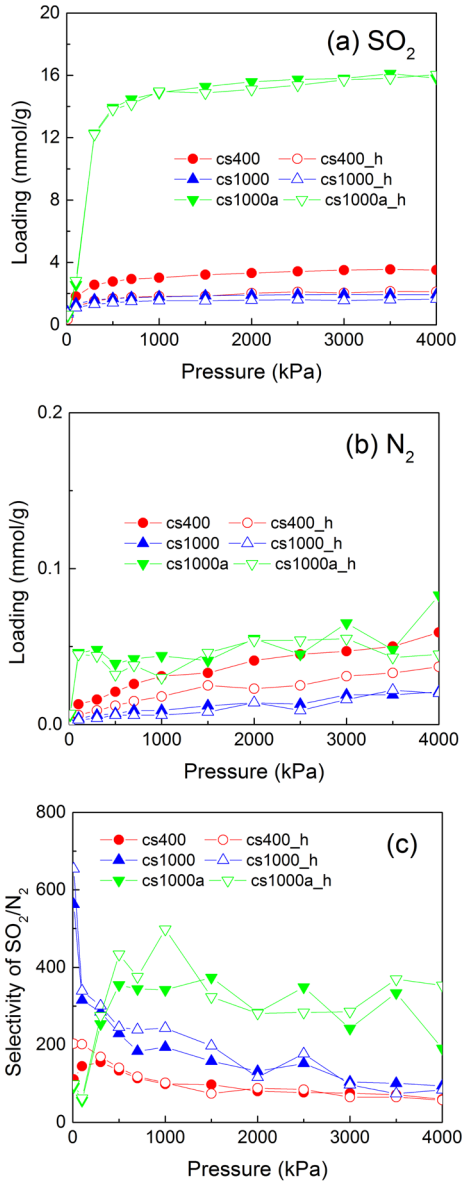

Figure 8. Adsorption isotherms and selectivity of equimolar N_2−SO_2 mixture at 303 K.

CO_2 is five to six times that of N_2. Here also the carbon−hydrogen models show greater selectivity than carbon-only models. This is due to the added dispersion interaction between hydrogen and gas molecules. The selectivity for cs1000/cs1000_h models varies between 20 and 25, which is greater than carbon nanotubes and CMK-5.[79,80] The adsorption isotherm for both CO_2 and N_2 increases with pressure; however, the CO_2 molecules preferentially adsorb at the surface and N_2 molecules adsorb in the space between the CO_2 molecules. For SO_2/N_2 system, cs1000a/cs1000a_h has the highest selectivity. This is due to the bigger pore size that can accommodate SO_2 molecules as compared with cs1000/cs400. The selectivity for cs1000 is ∼700 at very low pressures. This is due to the fact that at very low pressure only SO_2 molecules are adsorbed due to its high isosteric heat as compared with N_2 and thus the high selectivity. For SO_2/N_2 system, the selectivity is around 300−400 in cs1000a at moderate to high pressures, which is comparable to that with carbon nanotubes.[81] From Figure 8, it can been seen that the SO_2 molecules are saturated by 300 kPa, and further increase in pressure does not increase the amount of SO_2. However, the adsorption of N_2 is an increasing function of pressure. This is because N_2 molecules can accommodate in the space between the SO_2 molecules. Thus the selectivity decreases at higher pressures. For SO_2/CO_2 system, cs1000a shows better selectivity (again due to its comparatively larger pore size that can accommodate SO_2 molecules). The selectivity is ∼20 at low pressure (more than that reported for carbon nanotubes at low pressures[81]) and monotonously decreases with pressure. The reason is that SO_2 molecules are saturated around 300 kPa and CO_2 molecules show an increase in adsorption amount as the pressure increases. Furthermore, these selectivities (for different gases) span several orders of magnitude from 2 to 700 for different pairs, which is strongly dependent on the types of the adsorbents and adsorbates. For the CO_2−N_2 system, the selectivity is 20−25 for cs1000/cs1000_h system, followed by cs400/cs400_h (selectivity is 8−12), followed by cs1000a/cs1000a_h (selectivity is 5−8). This shows that microporous carbons can

DOI: 10.1021/acs.jpcc.7b01925
J. Phys. Chem. C 2017, 121, 13457−13473

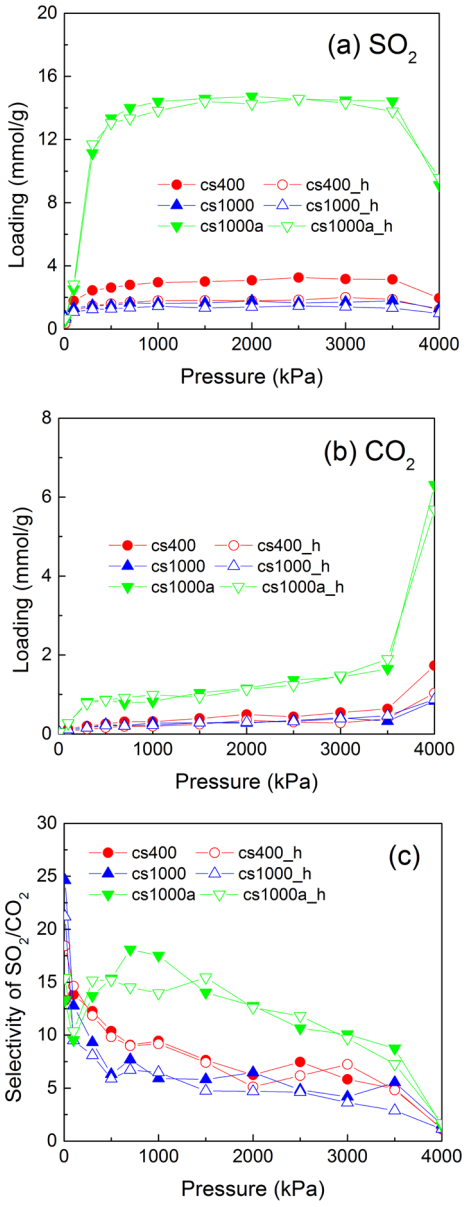

Figure 9. Adsorption isotherms and selectivity of equimolar CO_2−SO_2 mixture at 303 K.

be used as separation materials for CO_2−N_2 systems. Again, the selectivity for N_2−SO_2 is highest for cs1000a/cs1000a_h with a value of ∼400 at medium to high pressures. Interestingly, cs1000/cs1000_h and cs400/cs400_h show a monotonously decreasing function for selectivity for N_2−SO_2 systems. cs1000/cs1000_h materials have a selectivity of ∼700 at low pressures and fall to ∼100 at high pressures. cs1000a/cs1000a_h also have higher selectivity for CO_2/SO_2 systems. Thus cs1000a/cs1000a_h materials can be used for the separation of N_2−SO_2 and CO_2/SO_2 systems. For the cs1000a_h material that has the greatest loadings, the selectivities of CO_2 in CH_4−CO_2 and N_2−CO_2 systems are 2.43 and 5.95 at 4000 kPa, which is very close to the 2.9 and 5.4 at 298 K and 4000 kPa for a member of mesoporous materials UMCM-1 MOF.[82] As we show in the next section, the selectivity of CO_2 can be enhanced by incorporating functional groups to the carbon matrix.

Effect of Carbonyl Functional Groups on Separation of Binary Mixtures. We investigated the effect of carbonyl functional groups on the separation of gases for all three carbon samples. Figure 10 shows the selectivity of different binary gaseous systems in the carbon models with attached functional groups. From Figure 10a, we can see that for CH_4/CO_2 system cs1000_84 has the highest selectivity. The selectivity is around 4 to 5 for cs1000 without functional groups (see Figure 5c), and the selectivity increases to around 20−40 across pressures for cs1000_84. cs400_140 has the second highest selectivity around 10−15. Interestingly, cs1000_84 has higher selectivity than cs400_140, which has the highest number of attached functional groups. However, cs400 has a lower density than cs1000. This shows that the density of carbon samples also plays a major role in addition to the attached functional groups in determining the selectivity of gases. For SO_2/CO_2 system the selectivities increase only slightly on adding functional groups. For the carbon samples without functional groups, cs1000a/cs1000a_h have the highest selectivities and the selectivities have the decreasing function with pressure (see Figure 9c). On adding functional groups we find that cs1000a_28 has the highest selectivity. This shows that functional groups have no significant effect on the separation of SO_2/CO_2 system. cs1000_84 and cs400_140 have selectivities lower than cs1000a_28 system. For CH_4/N_2 system, the selectivities are of similar values for all carbon samples with and without functional groups. This shows that the functional groups do not have much effect on selectivities of CH_4/N_2 system, which is expected, as these gases are nonpolar gases. For CO_2/N_2 system, cs1000_84 has the highest selectivity. The selectivity varied from 20 to 25 without functional groups (see Figure 7c) but varied from 100 to 170 with attached functional groups. The selectivities are high for pressures up to 2000 kPa. At high pressures the selectivity decreases. This is due to the fact that at low pressures CO_2 is preferentially adsorbed, and as pressure increases N_2 molecules are adsorbed in the space between CO_2 and thus results in decrease in selectivity. The selectivities increases for all the carbon samples with attached functional groups as compared to pristine carbon samples. For SO_2/N_2 system, the selectivity with attached functional groups shows a decreasing function of pressure for cs1000_84 and cs400_140. The selectivities increase around 10-fold with attached functional groups compared with those of pristine carbons without attached functional groups. cs1000_84 and cs400_140 have the highest selectivities for SO_2/N_2 system. At very low pressure, only SO_2 molecules are adsorbed, and so there is a spike in selectivity. At pressures until 1500 kPa, cs1000_84 and cs400_140 have the highest selectivities, but at pressures above 2000 kPa, cs1000a_28 also has selectivities similar to that seen for cs400_140 and cs1000_84. It should be noted that cs1000 and cs400 show enhanced selectivity for SO_2 on addition of functional groups. cs400 and cs1000 have smaller pore size, and on addition of functional groups, SO_2 is preferentially adsorbed, and thus they show more selectivity for SO_2/N_2 as compared with cs1000a (which has a larger pore volume and larger pore sizes) at low pressures. Here also the selectivity shows a monotonous decrease with respect to pressure as SO_2 adsorption is saturated around 300 kPa and N_2 adsorption increases, as it fills the gap between SO_2 molecules.

Figure 11 shows the adsorption isotherms of preferential adsorbed species in the carbon models with attached functional groups. Despite the smallest number of functional groups, the loadings of preferential adsorbed species are the largest for cs1000a_28, arising from the greatest pore volume. Furthermore, for CH_4−CO_2, N_2−CH_4, and N_2−CO_2 systems, the

DOI: 10.1021/acs.jpcc.7b01925
J. Phys. Chem. C 2017, 121, 13457−13473

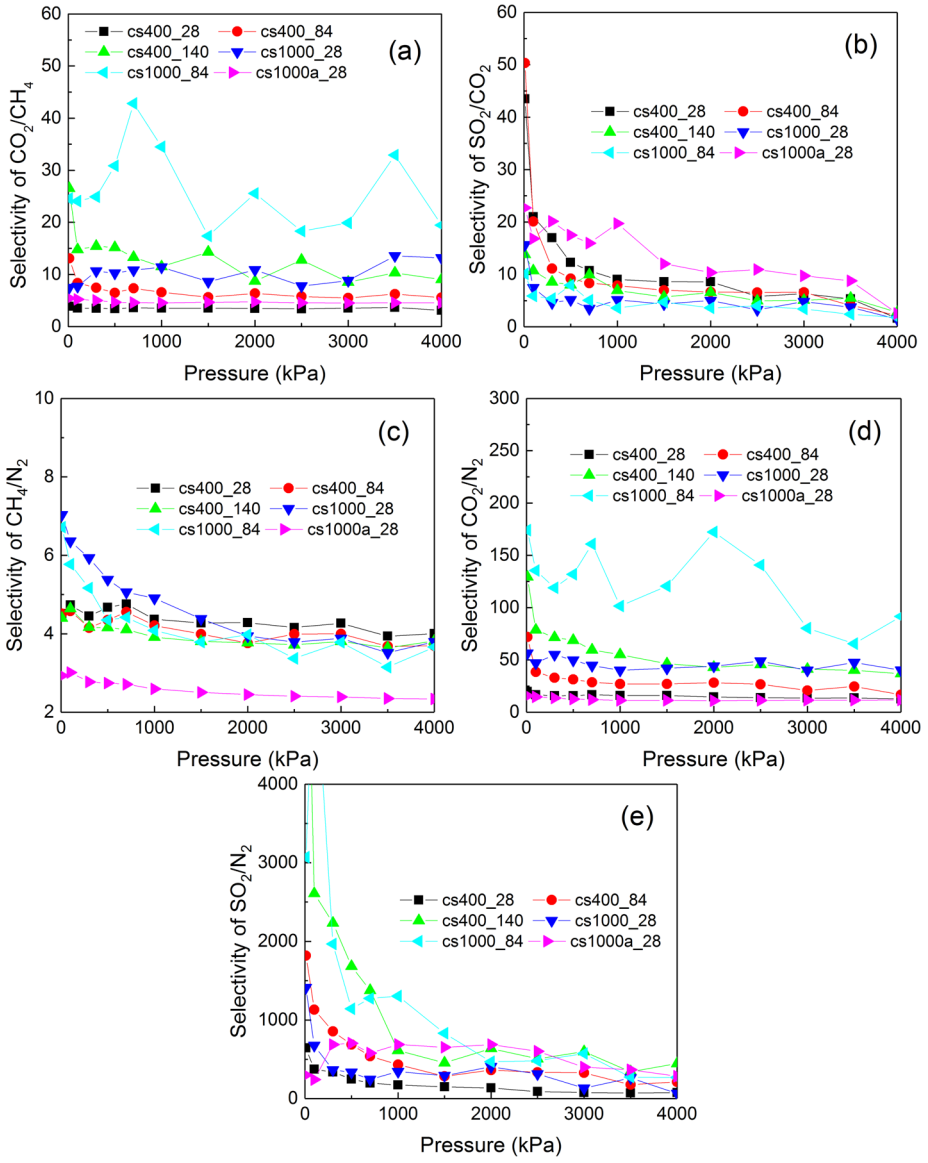

Figure 10. Adsorption selectivity of equimolar mixture at 303 K for cs400, cs1000, and cs1000a decorated by different numbers of carbonyl functional groups.

adsorption isotherms in cs1000a_28 exhibit a monotonic increasing with pressure, while for CO_2−SO_2 and N_2−SO_2 systems, there is a sudden jump of loading at the pressure of 200−300 kPa, which indicates the cooperative filling of SO_2 molecules in the wide micropores of cs1000a_28. Different from N_2−SO_2 system, the loading of SO_2 decreases for CO_2−SO_2 system at the pressures >3500 kPa. This is because CO_2 produces the stronger competitive adsorption effect with SO_2 molecules. The loadings of SO_2 in cs1000a_28 are ∼14 mmol/g for both systems. It means cs1000a_28 is an excellent separation adsorbent for SO_2 removal due to high loading and high selectivity of SO_2.

Effect of Carboxyl Functional Groups on Separation of Binary Mixtures. Figure 12 shows the selectivities of SO_2/CO_2, CO_2/N_2, and SO_2/N_2 in carbon materials decorated by different numbers of carboxyl functional groups. We can see that the selectivity of SO_2/CO_2 mixture shows fluctuating trends for cs1000a_24cooh and decreases at high pressures (∼4000 kPa). cs1000a_24cooh shows higher selectivities compared with the rest of the cases. This was also seen for carbonyl functional groups. This is because cs1000a has higher pore sizes. Interestingly, the selectivity of cs1000_23cooh decreases for lower to moderate pressures (up to 2000 kPa) and then increases and eventually decreases at higher pressures (at 4000 kPa). Also, the cs400_28cooh shows higher selectivity than cs400_48cooh. This might be because of smaller pores in cs400 that cannot be accessed by SO_2 molecules due to the addition of the functional groups (decreasing the pore size). For approximately the same number of functional groups, the −COOH functional groups show slightly higher selectivities for SO_2/CO_2 mixtures than the carbonyl functional groups.

Selectivity of CO_2/N_2 mixtures in −COOH functional groups shows a decreasing trend. cs400_48cooh shows the maximum selectivity in all four cases studied here. The trend is cs400_48cooh > cs1000_23cooh > cs400_28cooh > cs1000a_24cooh. At the pressure of 2000 kPa, cs1000_23cooh shows a maximum and more selectivity than cs400_48cooh. Otherwise, the trend is decreasing for all cases. For approximately the same number of functional groups, the −COOH

DOI: 10.1021/acs.jpcc.7b01925
J. Phys. Chem. C 2017, 121, 13457−13473

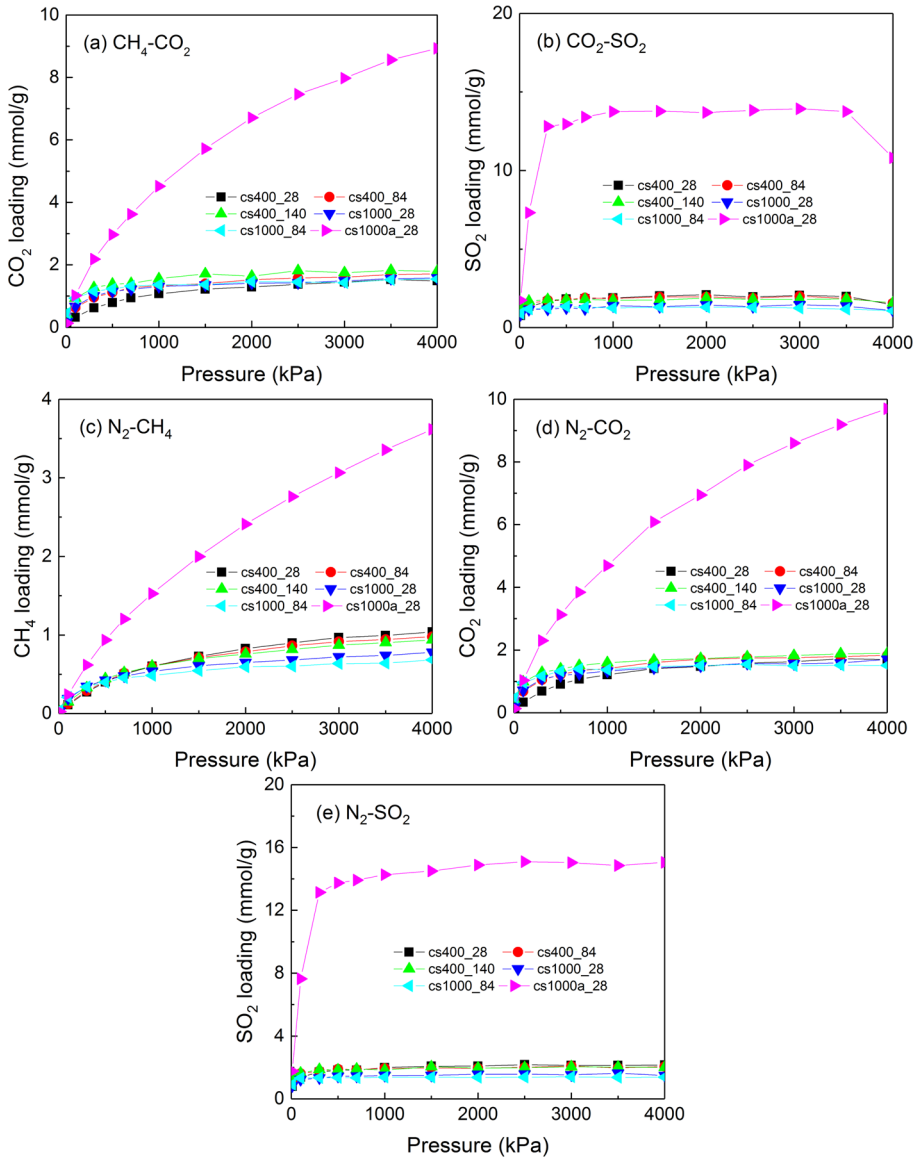

Figure 11. Adsorption isotherms of preferential adsorbed species in equimolar mixture at 303 K for cs400, cs1000, and cs1000a decorated by different numbers of carbonyl functional groups.

functional groups show higher selectivities for CO_2/N_2 mixtures than the carbonyl functional groups.

Selectivity of SO_2/N_2 mixtures in −COOH functional groups shows fluctuating trends for cs1000a_24cooh. For cs1000_23cooh, the selectivity shows a fluctuating trend until pressure = 1000 kPa and decreasing trend thereafter. For cs400_48cooh, the selectivity increases at low pressure and decreases for moderate and high pressures. Interestingly, at very low pressure, cs1000_23cooh shows higher selectivities, and for moderate to high pressure, cs1000a_24cooh shows higher selectivities. For approximately the same number of functional groups, the −COOH functional groups show higher selectivities for SO_2/N_2 mixtures than the carbonyl functional groups.

Comparison of GCMC Simulations and IAST Predictions for N_2−CO_2 Adsorption. We predicted the adsorption of equimolar N_2/CO_2 mixture by IAST modeling and compared the results with those from GCMC simulations. Figure 13a shows the fitting of GCMC simulations of pure gases by DSLF model, and Table 3 gives the fitted DSLF parameters. From Figure 13a and Table 3, we see that the fitting of DSLF model is excellent because the average relative deviations (ARDs) are <6% for all pure gas isotherms. It indicates that the obtained DSLF parameters are suitable for IAST predictions. However, we fail to fit the adsorption isotherm of pure SO_2 gas. This is because the loading of SO_2 quickly reaches a saturated value at a low pressure, corresponding to micropore filling of a type-I isotherm. This isotherm shape is inappropriate to be described by the DSLF equation. Therefore, we only present the results of N_2/CO_2 system. Figure 13b,c shows the comparison of IAST predictions with GCMC simulations for mixture adsorption. For cs1000a without functional groups, the adsorption isotherms and the selectivities by IAST prediction agree well with the GCMC results. However, for cs1000a_24cooh that has COOH functional groups, IAST predicted the selectivities of CO_2/N_2 about 15−35 higher than the GCMC results at the investigated pressure ranges. This inconsistency of both methods in the cs1000a_24cooh case is due to the existence of strong interactions between COOH functional groups and CO_2 molecules.

DOI: 10.1021/acs.jpcc.7b01925
J. Phys. Chem. C 2017, 121, 13457−13473

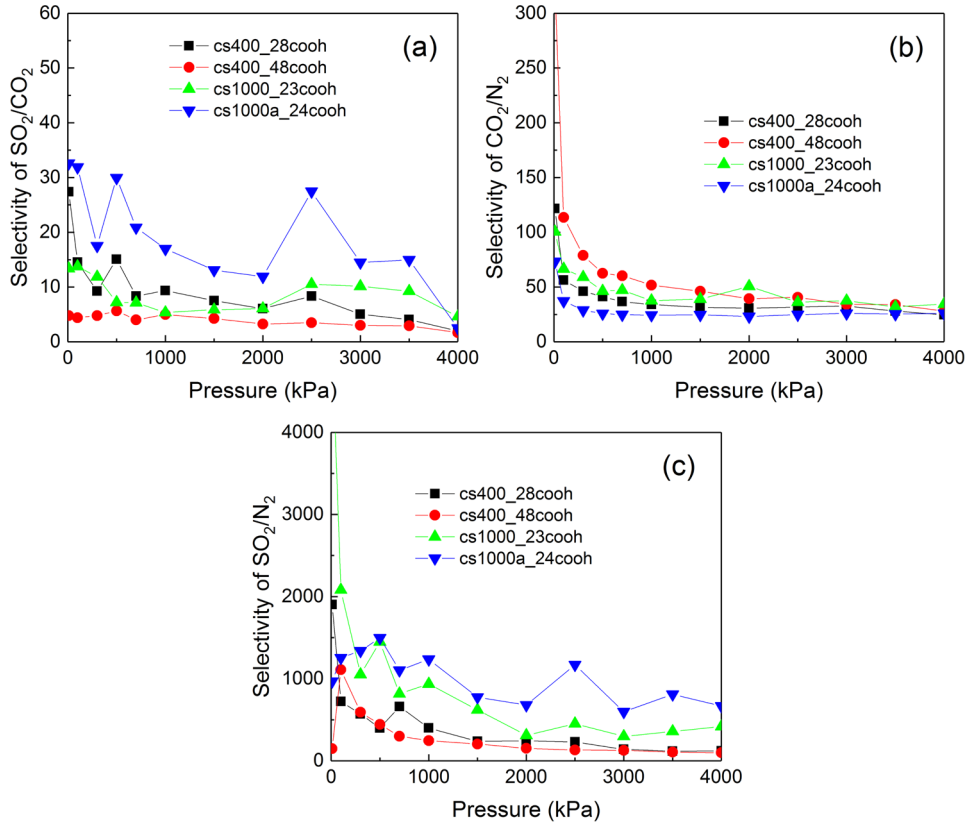

Figure 12. Adsorption selectivity of equimolar N_2−CO_2, CO_2−SO_2, and N_2−SO_2 mixtures at 303 K for cs400, cs1000, and cs1000a decorated by different numbers of carboxyl functional groups.

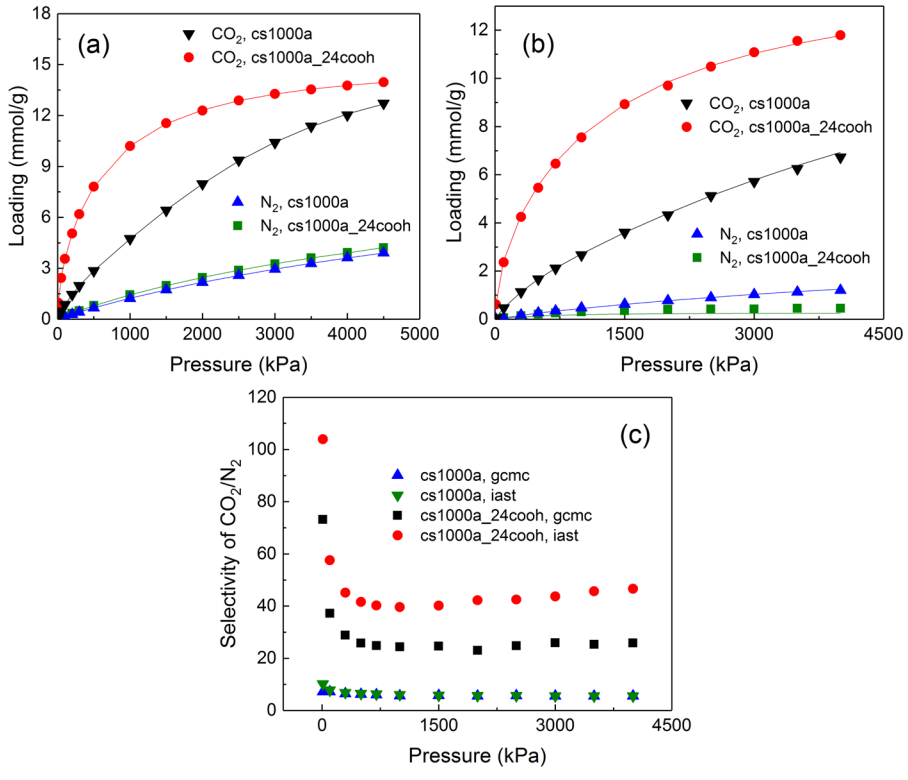

Figure 13. Adsorption loading and selectivity of CO_2/N_2 system in cs1000a and cs1000a_24cooh that decorated by 24 carboxyl functional groups at 303 K. (a) Pure CO_2 and N_2 adsorption isotherms. The lines are fits of the dual-site Langmuir−Freundlich equation to GCMC simulation results. (b) Adsorption loadings of single-component for the equimolar N_2−CO_2 mixtures, where the solid symbols are the GCMC simulations and the lines are IAST predictions. (c) Adsorption selectivities of CO_2/N_2 for the equimolar mixtures from GCMC simulations and IAST predictions.

DOI: 10.1021/acs.jpcc.7b01925
J. Phys. Chem. C 2017, 121, 13457−13473

Table 3. Parameters of Dual-Site Langmuir−Freundlich Equation by Fitting Absolute Adsorption Isotherms at 303 K from GCMC Simulations

adsorbent	adsorbate	N_1	k_1	n_1	N_2	k_2	n_2	ARD[a]
cs1000a	N_2	3.4748	0.4166	1.0085	5.3664	0.0415	1.587	3.05
	CO_2	9.6041	0.1079	2.2810	9.1575	0.7710	0.8823	5.25
cs1000a_24cooh	N_2	5.8323	0.069	1.4334	2.8021	0.6156	1.0144	2.79
	CO_2	9.107	1.1935	1.1952	7.0928	3.3012	0.676	0.82

[a]ARD is the average relative deviation (%) of fitted results from GCMC simulations.

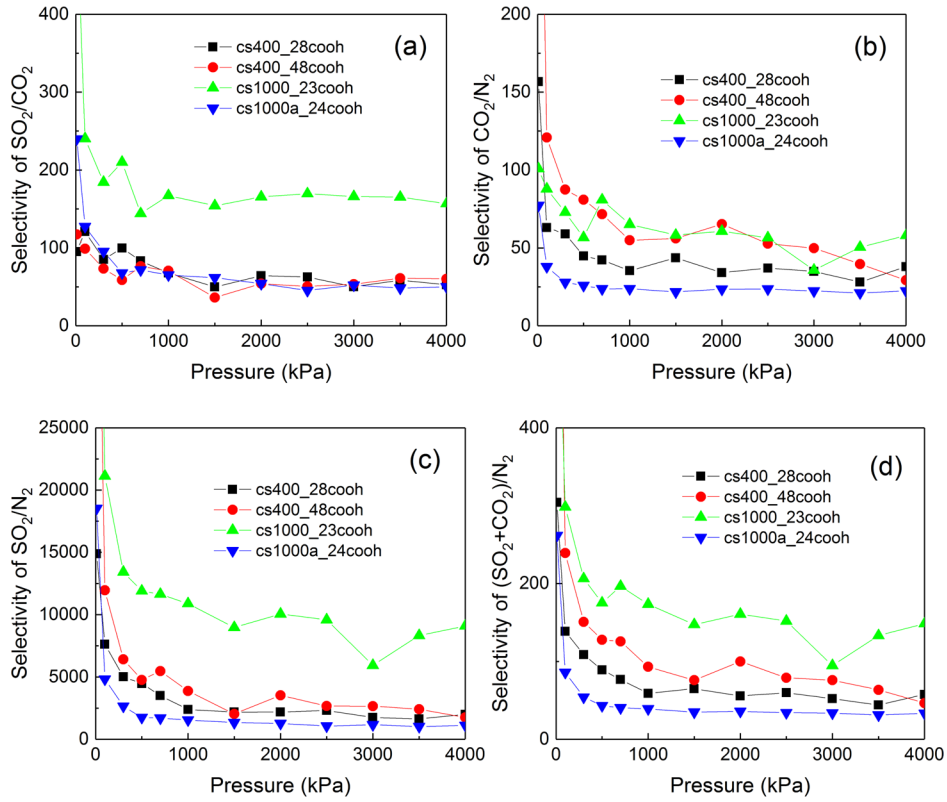

Figure 14. Adsorption selectivities of preferential adsorbed species in $N_2/CO_2/SO_2$ ternary mixture (gas composition of yN_2:yCO_2:ySO_2 = 0.8:0.198:0.002) at 303 K for cs400, cs1000, and cs1000a materials decorated by different numbers of carboxyl functional groups.

Even so, IAST predicted a similar variation trend of the selectivities as the GCMC results. Consequently, we should be cautious to apply IAST for quantitative description of the adsorption systems that possess strong polarity characteristics. However, IAST may be used in qualitative prediction for such case.

Effect of Carboxyl Functional Groups on Separation of Ternary Mixtures. In recent studies of graphene nanoribbons with edge functionalized[63] and CNT bundles,[81] the authors found that the selectivity of SO_2/N_2 shows improvement in $SO_2/CO_2/N_2$ ternary mixtures as compared with SO_2/N_2 binary mixtures. It will be nice to study ternary mixtures in our carbon models and see how the selectivites compare with the graphene and CNT bundles. Therefore, we performed the GCMC simulations for $N_2/CO_2/SO_2$ ternary mixture with a bulk concentration of yN_2 = 0.8 and ySO_2 = 0.002. As shown in Figure 14, selectivity of SO_2/CO_2 is higher in ternary mixture of $SO_2/CO_2/N_2$ than binary mixtures of SO_2/CO_2 for all of the cases studied here. Interestingly, cs1000_23cooh has the highest selectivity of all of the cases. In the binary case, cs1000a_24cooh shows the highest selectivity among all of the samples. Selectivity of CO_2/N_2 in ternary mixtures does not vary much from the binary mixtures. The trend in selectivities is roughly the same as that of binary CO_2/N_2 mixtures. This shows that the presence of SO_2 does not have much effect on CO_2/N_2 separation. Selectivity of SO_2/N_2 is higher in ternary mixtures as compared with the binary mixtures. Here also cs1000_23cooh shows the highest selectivity as compared with other samples. In binary SO_2/N_2 case, cs1000a_24cooh shows higher selectivity at moderate to higher pressures. Overall, our observation are consistent with the enhanced selectivity of SO_2/N_2 in ternary mixtures found by Maurya et al.[63] and Rahimi et al.[81]

CONCLUSIONS

We have studied adsorption and separation of gases in realistic molecular models of three porous carbon samples. Molecular models of carbons were developed using a HRMC method, which captures the pore topology and morphology actually present in real porous carbon materials. The pore size of cs400 and cs1000 models spans from 0.34 to 0.7 nm, and that of cs1000a spans to 1.2 nm. cs1000a/cs1000a_h system shows maximum uptake for all gases studied. This is because the pore volume of cs1000a is maximum. The isosteric heat of

DOI: 10.1021/acs.jpcc.7b01925
J. Phys. Chem. C 2017, 121, 13457−13473

adsorption for all the gases considered in this work was larger for cs1000/cs1000_h models at low pressure. This is because the carbon density of cs1000 is the highest. We found that cs1000 sample (with highest carbon density) shows the largest separation ability for N_2/CH_4, CH_4/CO_2, and N_2/CO_2 systems. cs1000a sample (with comparatively larger pore size) shows higher selectivity for SO_2/N_2 and SO_2/CO_2 systems. This shows that the SO_2-containing system displays better separation ability for carbon samples with large pore widths (up to 1.2 nm studied in this work). The carbon models with hydrogen show marginally higher separation ability as compared with carbon-only models for all gases (except for the SO_2 system). We further studied the effect of functional groups on the separation ability of the carbon models by adding carbonyl and carboxyl functional groups to the carbon−hydrogen models of the three samples. Carboxyl functional groups show higher selectivities than carbonyl functional groups. We found that the presence of functional groups results in higher selection abilities for all gases studied, except for the N_2/CH_4 system. This is expected because both N_2 and CH_4 are nonpolar gases. The separation ability of CO_2/N_2 and CO_2/CH_4 was enhanced for the carbon samples on adding functional groups, with cs1000 having the highest selectivity. Thus activated porous carbons with attached functional groups can be used to separate binary gas mixtures. The separation abilities of microporous carbons with attached functional groups are comparable to or better than carbon nanotubes for $CO_2/N_2/SO_2$ binary mixture considered in this work. The selectivity of the gases was observed in the following order: $SO_2/N_2 > CO_2/N_2 > SO_2/CO_2 > CO_2/CH_4 > CH_4/N_2$.

■ ASSOCIATED CONTENT

Supporting Information

The Supporting Information is available free of charge on the ACS Publications website at DOI: 10.1021/acs.jpcc.7b01925.

Pair correlation function (C−C) of cs400, cs1000, and cs1000a obtained from experiment and from the model. (PDF)

■ AUTHOR INFORMATION

Corresponding Author

*E-mail: pengxuan@mail.buct.edu.cn; pengxuan@126.com.

ORCID

Xuan Peng: 0000-0003-3220-7957

Jayant Kumar Singh: 0000-0001-8056-2115

Notes

The authors declare no competing financial interest.

■ ACKNOWLEDGMENTS

X.P. is grateful to the "CHEMCLOUDCOMPUTING" of BUCT for computational support and the National Natural Science Foundation of China (no. 21676006) for financial support. J.K.S is grateful to Ministry of Earth Science, Government of India for financial support (MOES/16/16/2013-RDEAS).

■ REFERENCES

(1) Gregg, S. J. S.; Sing, K. S. W. *Adsorption, Surface Area and Porosity*, 2nd ed.; Academic Press: London, 1982.

(2) Sircar, S.; Golden, T. C.; Rao, M. B. Activated carbon for gas separation and storage. *Carbon* **1996**, *34*, 1−12.

(3) Marsh, H.; Heintz, E. A.; Rodriguez-Reinoso, F. *Introduction to Carbon Technologies*; University of Alicante, 1997.

(4) Lipman, T. E.; DeLucchi, M. A. Hydrogen−fuelled vehicles. *Int. J. Vehicle Des.* **1996**, *17*, 562−589.

(5) Gadd, G. E.; Evans, P. J.; Kennedy, S.; James, M.; Elcombe, M.; Cassidy, D.; Moricca, S.; Holmes, J.; Webb, N.; Dixon, A.; Prasad, P. Gas storage in fullerenes. *Fullerene Sci. Technol.* **1999**, *7*, 1043−1143.

(6) Zhang, Z.; Yao, Z.; Xiang, S.; Chen, B. Perspective of microporous metal−organic frameworks for CO_2 capture and separation. *Energy Environ. Sci.* **2014**, *7*, 2868−2899.

(7) Rahimi, M.; Singh, J. K.; Babu, D. J.; Schneider, J. J.; Muller-Plathe, F. Understanding carbon dioxide adsorption in carbon nanotube arrays: molecular simulation and adsorption measurements. *J. Phys. Chem. C* **2013**, *117*, 13492−13501.

(8) Sayari, A.; Belmabkhout, Y.; Serna-Guerrero, R. Flue gas treatment via CO_2 adsorption. *Chem. Eng. J.* **2011**, *171*, 760−774.

(9) Littel, R. J.; Versteeg, G. F.; Van Swaaij, W. P. M. Physical absorption into non-aqueous solutions in a stirred cell reactor. *Chem. Eng. Sci.* **1991**, *46*, 3308−3313.

(10) Bishnoi, S.; Rochelle, G. T. Absorption of carbon dioxide into aqueous piperazine: reaction kinetics, mass transfer and solubility. *Chem. Eng. Sci.* **2000**, *55*, 5531−5543.

(11) Aroonwilas, A.; Veawab, A. Characterization and comparison of the CO_2 absorption performance into single and blended alkanolamines in a packed column. *Ind. Eng. Chem. Res.* **2004**, *43*, 2228−2237.

(12) Miller, B. G. *Fossil Fuel Emissions Control Technologies: Stationary Heat and Power Systems*, 1st ed.; Butterworth-Heinemann, 2015.

(13) He, B.; Zheng, X.; Wen, Y.; Tong, H.; Chen, M.; Chen, C. Temperature impact on SO_2 removal efficiency by ammonia gas scrubbing. *Energy Convers. Manage.* **2003**, *44*, 2175−2188.

(14) Stromberg, A. M.; Karlsson, H. T. Limestone based spray dry scrubbing of SO_2. *Chem. Eng. Sci.* **1988**, *43*, 2095−2102.

(15) van Dam, M. H. H.; Lamine, A. S.; Roizard, D.; Lochon, P.; Roizard, C. Selective sulfur dioxide removal using organic solvents. *Ind. Eng. Chem. Res.* **1997**, *36*, 4628−4637.

(16) Deng, R.; Jia, L.; Song, Q.; Su, S.; Tian, Z. Reversible absorption of SO_2 by amino acid aqueous solutions. *J. Hazard. Mater.* **2012**, *229*−*230*, 398−403.

(17) Tang, Z.; Zhou, C.; Chen, C. Studies on flue gas desulfurization by chemical absorption using an ethylenediamine−phosphoric acid solution. *Ind. Eng. Chem. Res.* **2004**, *43*, 6714−6722.

(18) Guo, J.; Lua, A. C. Microporous activated carbons prepared from palm shell by thermal activation and their application to sulfur dioxide adsorption. *J. Colloid Interface Sci.* **2002**, *251*, 242−247.

(19) Grzyb, B.; Albiniak, A.; Broniek, E.; Furdin, G.; Marêché, J. F.; Bégin, D. SO_2 adsorptive properties of activated carbons prepared from polyacrylonitrile and its blends with coal-tar pitch. *Microporous Mesoporous Mater.* **2009**, *118*, 163−168.

(20) Wang, W.; Peng, X.; Cao, D. P. Capture of trace sulfur gases from binary mixtures by single-walled carbon nanotube arrays: a molecular simulation study. *Environ. Sci. Technol.* **2011**, *45*, 4832−4838.

(21) Rahimi, M.; Babu, D. J.; Singh, J. K.; Yang, Y.; Schneider, J. J.; Muller-Plathe, F. Double-walled carbon nanotube array for CO_2 and SO_2 adsorption. *J. Chem. Phys.* **2015**, *143*, 124701.

(22) Srinivasan, A.; Grutzeck, M. W. The adsorption of SO_2 by zeolites synthesized from fly ash. *Environ. Sci. Technol.* **1999**, *33*, 1464−1469.

(23) Ivanova, E.; Koumanova, B. Adsorption of sulfur dioxide on natural clinoptilolite chemically modified with salt solutions. *J. Hazard. Mater.* **2009**, *167*, 306−312.

(24) Wang, X.; Ma, X.; Zhao, S.; Wang, B.; Song, C. Nanoporous molecular basket sorbent for NO_2 and SO_2 capture based on a polyethylene glycol-loaded mesoporous molecular sieve. *Energy Environ. Sci.* **2009**, *2*, 878−882.

(25) Xu, L.; Guo, J.; Jin, F.; Zeng, H. Removal of SO_2 from O_2-containing flue gas by activated carbon fiber (ACF) impregnated with NH_3. *Chemosphere* **2006**, *62*, 823−826.

(26) Mochida, I.; Korai, Y.; Shirahama, M.; Kawano, S.; Hada, T.; Seo, Y.; Yoshikawa, M.; Yasutake, A. Removal of SO_x and NO_x over activated carbon fibers. *Carbon* **2000**, *38*, 227−239.
(27) Fernandez, C. A.; Thallapally, P. K.; Motkuri, R. K.; Nune, S. K.; Sumrak, J. C.; Tian, J.; Liu, J. Gas-Induced expansion and contraction of a fluorinated metal−organic framework. *Cryst. Growth Des.* **2010**, *10*, 1037−1039.
(28) Yang, S.; Sun, J.; Ramirez-Cuesta, A. J.; Callear, S. K.; David, W. I.; Anderson, D. P.; Newby, R.; Blake, A. J.; Parker, J. E.; Tang, C. C.; Schröder, M. Selectivity and direct visualization of carbon dioxide and sulfur dioxide in a decorated porous host. *Nat. Chem.* **2012**, *4*, 887−894.
(29) Deng, W. Q.; Xu, X.; Goddard, W. A. New alkali doped pillared carbon materials designed to achieve practical reversible hydrogen storage for transportation. *Phys. Rev. Lett.* **2004**, *92*, 166103.
(30) Rahimi, M.; Singh, J. K.; Muller-Plathe, F. CO_2 adsorption on charged carbon nanotube arrays: a possible functional material for electric swing adsorption. *J. Phys. Chem. C* **2015**, *119*, 15232−15239.
(31) Plaza, G. M.; Garcia, S.; Rubiera, F.; Pis, J. J.; Pevida, C. Post-combustion CO_2 capture with a commercial activated carbon: comparison of different regeneration strategies. *Chem. Eng. J.* **2010**, *163*, 41−47.
(32) Wang, Q.; Luo, J.; Zhong, Z.; Borgna, A. CO_2 capture by solid adsorbents and their applications: current status and new trends. *Energy Environ. Sci.* **2011**, *4*, 42−55.
(33) Millward, A. R.; Yaghi, O. M. Metal−organic frameworks with exceptionally high capacity for storage of carbon dioxide at room temperature. *J. Am. Chem. Soc.* **2005**, *127*, 17998−17999.
(34) Yang, Q.; Zhong, C.; Chen, J. F. Computational study of CO_2 storage in metal−organic frameworks. *J. Phys. Chem. C* **2008**, *112*, 1562−1569.
(35) Banerjee, R.; Furukawa, H.; Britt, D.; Knobler, D.; O'Keeffe, M.; Yaghi, O. M. Control of pore size and functionality in isoreticular zeolitic imidazolate frameworks and their carbon dioxide selective capture properties. *J. Am. Chem. Soc.* **2009**, *131*, 3875−3877.
(36) Caskey, S. R.; Wong-Foy, A. G.; Matzger, A. J. Dramatic tuning of carbon dioxide uptake via metal substitution in a coordination polymer with cylindrical pores. *J. Am. Chem. Soc.* **2008**, *130*, 10870−10871.
(37) Shan, M.; Xue, Q.; Jing, N.; Ling, C.; Zhang, T.; Yan, Z.; Zheng, J. Influence of chemical functionalization on the CO_2/N_2 separation performance of porous graphene membranes. *Nanoscale* **2012**, *4*, 5477−5482.
(38) Kurniawan, K.; Bhatia, S. K.; Rudolph, V. Simulation of binary mixture adsorption of methane and CO_2 at supercritical conditions in carbons. *AIChE J.* **2006**, *52*, 957−967.
(39) Furmaniak, S.; Kowalczyk, P.; Terzyk, A. P.; Gauden, P. A.; Harris, P. J. F. Synergetic effect of carbon nanopore size and surface oxidation on CO_2 capture from CO_2/CH_4 mixtures. *J. Colloid Interface Sci.* **2013**, *397*, 144−153.
(40) Keskin, S.; Sholl, D. S. Assessment of a metal−organic framework membrane for gas separations using atomically detailed calculations: CO_2, CH_4, N_2, H_2 mixtures in MOF-5. *Ind. Eng. Chem. Res.* **2009**, *48*, 914−922.
(41) Liu, B.; Smit, B. Comparative molecular simulation study of CO_2/N_2 and CH_4/N_2 separation in zeolites and metal−organic frameworks. *Langmuir* **2009**, *25*, 5918−5926.
(42) Babarao, R.; Hu, Z. Q.; Jiang, J. W.; Chempath, S.; Sandler, S. I. Storage and separation of CO_2 and CH_4 in silicalite, C_{168} schwarzite, and IRMOF-1: a comparative study from Monte Carlo simulation. *Langmuir* **2007**, *23*, 659−666.
(43) Babarao, R.; Jiang, J. W. Unprecedentedly high selective adsorption of gas mixtures in rho zeolite-like metal−organic framework: a molecular simulation study. *J. Am. Chem. Soc.* **2009**, *131*, 11417−11425.
(44) Peng, X.; Wang, W. C.; Xue, R. S.; Shen, Z. M. Adsorption separation of CH_4/CO_2 on mesocarbon microbeads: experiment and modelling. *AIChE J.* **2006**, *52*, 994−1003.
(45) Peng, X.; Zhao, J. S.; Cao, D. P. Adsorption of carbon dioxide of 1-site and 3-site models in pillared clays: A Gibbs ensemble Monte Carlo simulation. *J. Colloid Interface Sci.* **2007**, *310*, 391−401.
(46) Jorge, M.; Schumacher, C.; Seaton, N. A. Simulation study of the effect of the chemical heterogeneity of activated carbon on water adsorption. *Langmuir* **2002**, *18*, 9296−9306.
(47) Birkett, G. R.; Do, D. D. The adsorption of water in finite carbon pores. *Mol. Phys.* **2006**, *104*, 623−637.
(48) Brennan, J. K.; Thomson, K. T.; Gubbins, K. E. Adsorption of water in activated carbons: effects of pore blocking and connectivity. *Langmuir* **2002**, *18*, 5438−5447.
(49) Liu, J. C.; Monson, P. A. Monte Carlo simulation study of water adsorption in activated carbon. *Ind. Eng. Chem. Res.* **2006**, *45*, 5649−5656.
(50) Dasgupta, T.; Punnathanam, S. N.; Ayappa, K. G. Effect of functional groups on separating carbon dioxide from CO_2/N_2 gas mixtures using edge functionalized graphene nanoribbons. *Chem. Eng. Sci.* **2015**, *121*, 279−291.
(51) Jain, S. K.; Pellenq, R. J. M.; Pikunic, J. P.; Gubbins, K. E. Molecular modeling of porous carbons using the hybrid reverse Monte Carlo method. *Langmuir* **2006**, *22*, 9942−9948.
(52) Jain, S. K.; Gubbins, K. E.; Pellenq, R. J. M.; Pikunic, J. P. Molecular modeling and adsorption properties of porous carbons. *Carbon* **2006**, *44*, 2445−2451.
(53) Coasne, B.; Jain, S. K.; Gubbins, K. E. Adsorption, structure and dynamics of fluids in ordered and disordered models of porous carbons. *Mol. Phys.* **2006**, *104*, 3491−3499.
(54) Billemont, P.; Coasne, B.; De Weireld, G. Adsorption of carbon dioxide-methane mixtures in porous carbons: effect of surface chemistry. *Adsorption* **2014**, *20*, 453−463.
(55) Jain, S. K.; Pikunic, J. P.; Pellenq, R. J. M.; Gubbins, K. E. Effects of activation on the structure and adsorption properties of a nanoporous carbon using molecular simulation. *Adsorption* **2005**, *11*, 355−360.
(56) Farmahini, A. H.; Bhatia, S. K. Hybrid Reverse Monte Carlo simulation of amorphous carbon: distinguishing between competing structures obtained using different modeling protocols. *Carbon* **2015**, *83*, 53−70.
(57) Liu, L.; Nicholson, D.; Bhatia, S. K. Adsorption of CH_4 and CH_4/CO_2 mixtures in carbon nanotubes and disordered carbons: A molecular simulation study. *Chem. Eng. Sci.* **2015**, *121*, 268−278.
(58) Birkett, G. R.; Do, D. D. Simulation study of water adsorption on carbon black: the effect of graphite water interaction strength. *J. Phys. Chem. C* **2007**, *111*, 5735−5742.
(59) Lodewyckx, P.; Vansant, E. F. Water isotherms of activated carbons with small amounts of surface oxygen. *Carbon* **1999**, *37*, 1647−1649.
(60) Liu, Y.; Wilcox, J. Molecular simulation studies of CO_2 adsorption by carbon model compounds for carbon capture and sequestration applications. *Environ. Sci. Technol.* **2013**, *47*, 95−101.
(61) Lu, X.; Jin, S.; Wei, S.; Zhang, M.; Zhu, Q.; Shi, X.; Deng, Z.; Guo, W.; Shen, W. Competitive adsorption of a binary CO_2−CH_4 mixture in nanoporous carbons: effects of edge-functionalization. *Nanoscale* **2015**, *7*, 1002−1012.
(62) Gotzias, A.; Tylianakis, E.; Froudakis, G.; Steriotis, T. Adsorption in micro and mesoporous slit carbons with oxygen surface functionalities. *Microporous Mesoporous Mater.* **2015**, *209*, 141−149.
(63) Maurya, M.; Singh, J. K. A grand canonical Monte Carlo study of SO_2 capture using functionalized bilayer graphene nanoribbons. *J. Chem. Phys.* **2017**, *146*, 044704.
(64) Billemont, P.; Coasne, B.; De Weireld, G. Adsorption of carbon dioxide, methane, and their mixtures in porous carbons: effect of surface chemistry, water content, and pore disorder. *Langmuir* **2013**, *29*, 3328−3338.
(65) Halder, P.; Maurya, M.; Jain, S. K.; Singh, J. K. Understanding adsorption of CO_2, N_2, CH_4 and their mixtures in functionalized carbon nanopipe arrays. *Phys. Chem. Chem. Phys.* **2016**, *18*, 14007−14016.

DOI: 10.1021/acs.jpcc.7b01925
J. Phys. Chem. C 2017, 121, 13457−13473

(66) Furmaniak, S.; Terzyk, A. P.; Gauden, P. A.; Kowalczyk, P.; Szymanski, G. S. Influence of activated carbon surface oxygen functionalities on SO_2 physisorption − simulation and experiment. *Chem. Phys. Lett.* **2013**, *578*, 85−91.
(67) Peng, X.; Cao, D. P. Computational screening of porous carbons, zeolites, and metal organic frameworks for desulfurization and decarburization of biogas, natural gas, and flue gas. *AIChE J.* **2013**, *59*, 2928−2942.
(68) Zeng, Y.; Prasetyo, L.; Nguyen, V.; Horikawa, T.; Do, D.; Nicholson, D. Characterization of oxygen functional groups on carbon surfaces with water and methanol adsorption. *Carbon* **2015**, *81*, 447−457.
(69) Ni, B.; Lee, K.; Sinnott, S. B. A reactive empirical bond order (REBO) potential for hydrocarbon−oxygen interactions. *J. Phys.: Condens. Matter* **2004**, *16*, 7261−7275.
(70) Fonseca, A. F.; Lee, G.; Borders, T. L.; Zhang, H.; Kemper, T.; Shan, T.; Sinnott, S.; Cho, K. Reparameterization of the REBO-CHO potential for graphene oxide molecular dynamics simulations. *Phys. Rev. B: Condens. Matter Mater. Phys.* **2011**, *84*, 075460.
(71) Frenkel, D.; Smit, B. *Understanding Molecular Simulations*, 2nd ed.; Academic Press, 2002.
(72) Martin, M. G.; Siepmann, J. I. Transferable potentials for phase equilibria. 1. united-atom description of n-alkanes. *J. Phys. Chem. B* **1998**, *102*, 2569−2577.
(73) Potoff, J. J.; Siepmann, J. I. Vapor−liquid equilibria of mixtures containing alkanes, carbon dioxide, and nitrogen. *AIChE J.* **2001**, *47*, 1676−1682.
(74) Ribeiro, M. C. C. Molecular dynamics simulation of liquid sulfur dioxide. *J. Phys. Chem. B* **2006**, *110*, 8789−8797.
(75) Elliott, J. R.; Lira, C. T. *Introductory Chemical Engineering Thermodynamics*, 2nd ed.; Prentice-Hall, 1999.
(76) Peng, X.; Cao, D. P.; Wang, W. C. Computational study on purification of CO_2 from natural gas by C_{60} intercalated graphite. *Ind. Eng. Chem. Res.* **2010**, *49*, 8787−8796.
(77) Myers, A. L.; Prausnitz, J. M. Thermodynamics of mixed-gas adsorption. *AIChE J.* **1965**, *11*, 121−127.
(78) Vishnyakov, A.; Ravikovitch, P. I.; Neimark, A. V. Molecular level models for CO_2 sorption in nanopores. *Langmuir* **1999**, *15*, 8736−8742.
(79) Peng, X.; Cao, D. P.; Wang, W. C. Adsorption and separation of $CH_4/CO_2/N_2/H_2/CO$ mixtures in hexagonally ordered carbon nanopipes CMK-5. *Chem. Eng. Sci.* **2011**, *66*, 2266−2276.
(80) Kowalczyk, P. Molecular insight into the high selectivity of double-walled carbon nanotubes. *Phys. Chem. Chem. Phys.* **2012**, *14*, 2784−2790.
(81) Rahimi, M.; Singh, J. K.; Muller-Plathe, F. Adsorption and separation of binary and ternary mixtures of SO_2, CO_2 and N_2 by ordered carbon nanotube arrays: grand-canonical Monte Carlo simulations. *Phys. Chem. Chem. Phys.* **2016**, *18*, 4112−4120.
(82) Peng, X.; Cheng, X.; Cao, D. P. Computer simulations for the adsorption and separation of $CO_2/CH_4/H_2/N_2$ gases by UMCM-1 and UMCM-2 metal organic frameworks. *J. Mater. Chem.* **2011**, *21*, 11259−11270.

DOI: 10.1021/acs.jpcc.7b01925
J. Phys. Chem. C 2017, 121, 13457−13473